Proceedings of the ASME 2011 9th International Conference on Nanochannels, Microchannels, and Minichannels
ICNMM 2011
June 19-22, 2011, Edmonton, CANADA

ICNMM2011-58242

TWO-PHASE HEAT SINKS WITH MICROPOROUS COATING

Tadej Semenic
Advanced Cooling Technologies, Inc.
Lancaster, Pennsylvania, USA

Seung M. You
The University of Texas at Arlington
Dept. of Mechanical and Aerospace Engineering,
Box 19023 Arlington, Texas, USA

ABSTRACT

To minimize flow boiling instabilities in two-phase heat sinks, two different types of microporous coatings were developed and applied on mini- and small-channel heat sinks and tested using degassed R245fa refrigerant. The first coating was epoxy-based and was sprayed on heat sink channels while the second coating was formed by sintering copper particles on heat sink channels. Mini-channel heat sinks had overall dimensions 25.4 mm x 25.4 mm x 6.4 mm and twelve rectangular channels with a hydraulic diameter 1.7 mm and a channel aspect ratio of 2.7. Small-channel heat sinks had the same overall dimensions, but only three rectangular channels with hydraulic diameter 4.1 mm and channel aspect ratio 0.6. The microporous coatings were found to minimize parallel channel instabilities for mini-channel heat sinks and to reduce the amplitude of heat sink base temperature oscillations from 6 °C to slightly more than 1 °C. No increase in pressure drop or pumping power due to the microporous coating was measured. The mini-channel heat sinks with porous coating had in average 1.5-times higher heat transfer coefficient than uncoated heat sinks. Also, the small-channel heat sinks with the "best" porous coating had in average 2.5-times higher heat transfer coefficient and the critical heat flux was 1.5 to 2-times higher compared with the uncoated heat sinks.

INTRODUCTION

Flow boiling in micro-, mini-, and small-channel heat sinks offers several advantages over flow boiling in large-channel heat sinks in terms of reduced heat sink thermal resistance (i.e. reduced device temperature) and increased heat sink base heat flux. However, flow boiling instabilities and the resulting oscillations in pressure and heat sink base temperature limit the CHF condition (below the predicted value). Such oscillations can potentially cause structural failure not to mention that the device being cooled experiences large temperature swings that can adversely affect performance.

There exist several types or modes of flow boiling instabilities that are relevant to two-phase heat sinks. *Parallel channel* instabilities are closely related to *excursive* or *Ledinegg* instabilities [1] and may occur when the pressure drop-flow curve becomes smaller than the loop supply pressure drop-flow rate curve. *Compressible volume* instabilities [2] also can occur in systems that have a significant compressible volume upstream of the heated section. Bergles and Kandlikar [3] report that in micro-channel heat sinks, a small volume of subcooled liquid is sufficient to cause the compressible volume instability and lead to premature CHF. *Rapid bubble growth* [4, 5, 6, and 7] instability also occurs in channels with small hydraulic diameter. The initially spherical bubble which is confined in the spanwise direction (due to the presence of the channel walls) can only grow streamwise (downstream and upstream) which can cause flow reversal. As a result of this type of instability and the fact that not all the parallel channels nucleate bubbles at the same time, some channels are populated primarily with vapor while others with liquid, resulting in significant variation in the heat sink base temperature. *Critical heat flux* (CHF) instability is also well documented in Zuber [8]. Specifically related to flow boiling in micro- and mini-channels, the CHF refers to the outcome of the events that cause a sudden, appreciable decrease in the heat transfer coefficient or increase in the heat sink base temperature. Conditions that commonly affect the CHF instability include small mass flux, low inlet subcooling, and/or channels with a large length-to-diameter ratio. As discussed in Collier and Thome [9], the flow pattern at high heat fluxes near the channel outlet is mostly annular with the vapor phase occupying most of the channel core while the liquid flows as a thin film along the channel wall. Dryout of the liquid film near the outlet is widely regarded as the trigger mechanism for CHF.

Many authors have visualized different types of instabilities in multiple parallel micro- and mini-channel heat sinks. Kandlikar [10] visualized severe flow oscillations including flow reversal using water in an electrically heated evaporator consisting of six 1 mm x 1 mm large parallel channels. In some of the channels of the evaporator, the pressure drop across the channels was found to increase with vapor generation resulting in the decrease of the mass flow rate. As a result, the mass flow rate through other channels increased and led to instabilities. Hetsroni et al. [4, 5] tested several parallel triangular micro-channels with hydraulic diameters from 0.1 to 0.16 mm and number of channels from 17 to 26 using water. They observed that once bubble nucleation begins, the bubble grows rapidly and occupies the entire channel. The rapid bubble growth pushes the liquid-vapor interface on both caps of the vapor slug at the upstream and the downstream ends and leads to a reversed flow. After the bubble reaches the inlet or the outlet plenum, the channel gets rewetted and refilled with liquid. Not all the channels are rewetted and refilled with liquid at the same time resulting in large temperature differences across the heat sink. Qu and Mudawar [11, 12] have visualized compressible volume instabilities and parallel channel instabilities for 21 parallel micro-channels with channel width 215 µm and channel depth 821 µm. The compressible flow instability caused severe pressure drop oscillations across the heat sink. The parallel channel instabilities were intensified at a high heat flux and resulted in back flow of the vapor into the upstream plenum. Chang and Pan [6] tested a micro-channel heat sink with fifteen 99.4 µm wide and 76.3 µm deep parallel channels using DI water as working fluid. They observed forward and reverse slug or annular flow that appeared alternatively in every channel. Severe pressure oscillations were notices as well as the vapor flow in to the upstream plenum. Lee and Yao [13] conducted tests with DI water and 48 parallel micro-channels that were 0.235 mm wide and 0.71 mm deep. They have visualized long period cyclic fluctuations in heat sink temperature as well as the water inlet temperature. The oscillations in heat sink surface temperature of 15 °C were measured.

Parallel channel instabilities present in two-phase heat sinks may be reduced or eliminated by one the following means: (1) introducing a relatively large pressure drop at the inlet of each of the channels; (2) decreasing the superheat required for the onset of nucleate boiling inside the channels; or (3) physically separating the vapor phase from the two-phase mixture in the channels. Kandlikar [10] and Bergles and Kandlikar [3] predicted that by including an inlet restrictor before each channel, the parallel channel instabilities can be avoided. Koşar et al. [7], Agostini et al. [14], and Wang et al. [15] tested micro-channel heat sinks with integrated inlet slits and showed that the instabilities were suppressed. The penalty was an increased total pressure drop. In addition, the inlet slits (or restrictors) are very difficult to manufacture due to very small sizes. Furthermore, one restrictor design may not be effective across a wide range of operating conditions. Koşar et al. [16] and Kuo and Peles [17] used reentrant cavities on the micro-channel inner walls to decrease the nucleation superheat and consequently the instabilities. These reentrant cavities were formed on to the micro-channel walls using micromachining techniques. The cavities on microchannel walls were found to successfully delay the parallel channel instabilities and to increase the CHF. Although, the benefits of the cavities were demonstrated, the micromachining method is too expensive for high volume micro-channel heat sinks. David et al. [18] used a hydrophobic membrane to locally vent the vapor from a microchannel. This concept is limited to high surface tension fluids and becomes ineffective for many electronics cooling fluids that typically have low surface tension (e.g. refrigerants, dielectric fluids). Compressible volume instability can be suppressed by including an upstream throttling valve [11 and 12]. Rapid bubble growth instability can be minimized by increasing the channel size and decreasing the bubble departure diameter.

The objective of this paper is to minimize the parallel channel instabilities and the rapid bubble growth instability by developing heat sinks with microporous coating on channel walls. The microporous coating can reduce the incipient boiling superheat to start nucleating vapor bubbles, decrease the bubble departure diameter, and increase the channel heat transfer coefficient, thus allowing the use of heat sinks with larger hydraulic diameters.

NOMENCLATURE

w_{ch}	channel width (mm)
d_{ch}	channel depth (mm)
N_{ch}	number of channels

TEST ARTICLES

A heat sink model was developed to compute the heat transfer coefficient and the pressure drop across the heat sink channels for a given heat flux, coolant flow rate and heat sink geometry. The two-phase heat transfer coefficient was predicted using generalized Chen's correlation [19] and the Homogeneous Equilibrium Model was used to compute the two-phase pressure drops across the channels.

The model was used to determine a working fluid with most favorable thermophysical properties. It was also critical that the selected working fluid had a positive pressure at ambient temperatures as low as 15°C to ensure that no gases entered the test loop. R245fa refrigerant was selected as the working fluid.

The heat sink overall dimensions were 25.4 mm x 25.4 mm x 6.4 mm. The channel width for the first three heat sinks tested was 1.2 mm in part because previous work [20] successfully demonstrated that a microporous coating could be applied to 1 mm wide pin fins, which is approximately the same dimension as the channel size selected. The model was also used to evaluate different heat sinks with different channel depths and number of channels. The dependence of the heat sink base temperature on the channel depth and the number of channels for R245fa refrigerant are shown in Figure 1.

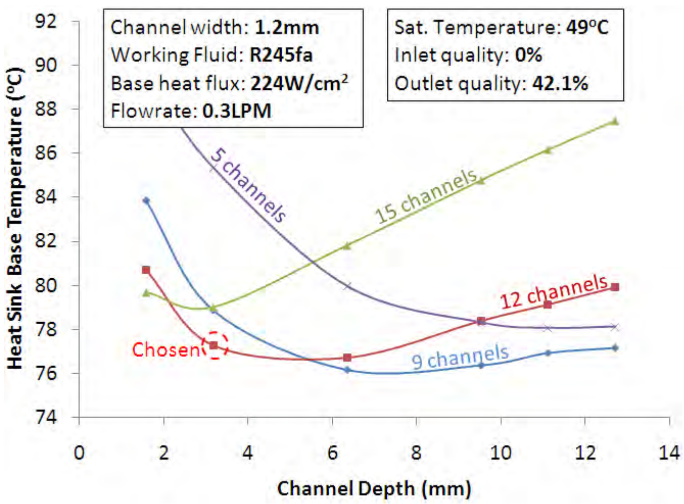

Figure 1: Heat sink base temperature versus channel depth for various heat sink designs

As the channel depth increases, the total cross-sectional area available for flow and the heat sink surface area increase; however, the heat sink surface efficiency and the average channel heat transfer coefficient decrease. For a low number of channels (e.g. 5 channels), very deep channels are needed to provide sufficient fin surface area. For a large number of channels (e.g. 15 channels), no improvement in performance is achieved by increasing the channel depth as shown in Figure 1, where the heat sink base temperature increases with increasing channel depth for the 12 and 15 channel cases. For reference, the fin thickness for 15 channels is only 0.3 mm resulting in high heat conduction resistance along the fins.

After reviewing various combinations of the number of channels and the channel depth, it was decided to design a heat sink with twelve 3.2 mm deep channels and 0.6 mm wide fins. The heat sink base thickness was decided to be 3.2 mm to ensure good heat sink base flatness and sufficient structural integrity of the heat sink. Two 2 mm thick fins were also designed on each side of the heat sink (peripheral fins) to further increase the structural integrity of the heat sink and to prevent heat sink deformation during clamping of the sightglass on top of the fins. In addition, a few more heat sinks were developed that had only three channels with channel width 5.8 mm and the same channel depth of 3.2 mm for further testing of the microporous coatings. Heat sink dimensions and the microporous coatings types applied on the heat sinks are summarized in Table 1.

You et al. [21] examined the effects of particle size on boiling performance of microporous enhanced surfaces using five different sizes of diamond particles and FC-72 working fluid. The results of their findings were that the incipient wall superheat to start nucleating vapor bubbles on microporous coatings with the particle size from 20 to 50 µm was 6-times lower than that for the plain surface. Based on these results, it was predicted that the optimal microporous coating for R245fa refrigerant and mini-channel heat sinks would have a particle diameter around 25 µm and be approximately 75-100 µm thick. Hsu's criteria predicted the most optimal cavity mouth radius for R245fa in the range from 5 to 15 µm. This cavity size corresponds to particle diameters from 10 to 40 µm.

Table 1: Heat sink parameters and microporous coating types

Heat Sink Test Sample	w_{ch} (mm)	d_{ch} (mm)	N_{ch}	Microporous Coating
1	1.2	3.2	12	none
2	1.2	3.2	12	ABM coating
3	1.2	3.2	12	Sintered coating 1
4	5.8	3.2	3	none
5	5.8	3.2	3	Sintered coating 1
6	5.8	3.2	3	Sintered coating 2
7	5.8	3.2	3	Sintered coating 3
8	5.8	3.2	3	ABM coating

The key requirements for the coating were uniform thickness, good adhesion, and good coverage. Two different approaches of porous coating fabrication and deposition methods were investigated. The first approach used an ABM (A=Aluminum particles, B=Brushable ceramic epoxy, M=Methyl ethyl ketone) coating [22] while the second approach formed a microporous coating by sintering copper particles on channel walls.

The ABM coating consists of particles, binder and carrier. The particles provide the structure material to create the required re-entrant cavities. The binder or glue binds the particles together and to a heating surface. Since the particles are solid and the binder is usually very viscous, a volatile carrier liquid is used to allow for adequate mixing of the particles and binder, and for application of the particles and binder to the surface. The carrier evaporates after applying the coating to the heated surface. The coating was deposited to the surface of the heat sinks by a spray coating method. The layer thickness was controlled within ~10 µm. For better uniformity of the coating thickness, the coating mixture was applied by spraying with compressed air. For a given average particle size of the aluminum powder, the final coating thickness was regulated by the time and number of passes with the spray gun over the area to be coated. After applying the coating to a test sample, the sample was sectioned, metallurgically mounted, and polished. The sample was inspected using an optical microscope and an SEM. After inspecting the quality of the coating, the coating bonding strength was also tested by immersing the heat sink coated with ABM coating in an ultrasonic bath. In the past, various durability tests were performed that included immersion of the coated sample for 4 days in an ultrasonic bath at 4 kHz frequency or use of the coated sample in a continuous boiling test at 15 W/cm2 for 110 hrs. In these tests, no particle loss or coating detachment was observed in SEM imaging. Therefore, the ABM microporous coating is securely attached to the surface and can be expected to be stable through multi-year service. A photograph of the ABM coating applied to a mini-channel heat sink is shown in Figure 2.

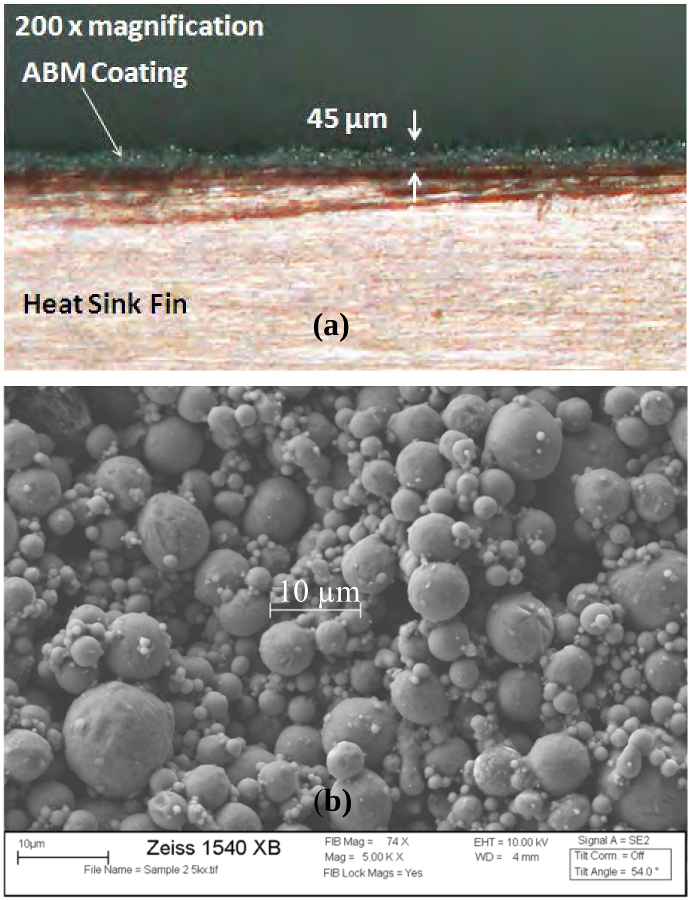

Figure 2: ABM microporous coating on a copper heat sink fin; (a) 200-times magnification, (b) 1540-times magnification

The thickness of the coating was approximately 45 µm. The average pore size of the coating ranges approximately from 2 to 10 µm.

The Sintered Coating was produced by bonding copper metal particles to a heat sink wall by solid state sintering. Sintering forms a strong metallurgical bond among the particles with very good adhesion to the base substrate. Three different variations of this coating were tested. Sintered coating 1 had approximately 5 to 15 µm large pores and was 35 µm thick; Sintered coating 2 had approximately 10 to 30 µm large pores and was 70 µm thick, and Sintered coating 3 had approximately 10 to 30 µm large pores and was 500 µm thick. A photograph of Sintered coating 1 on the heat sink fin is shown in Figure 3.

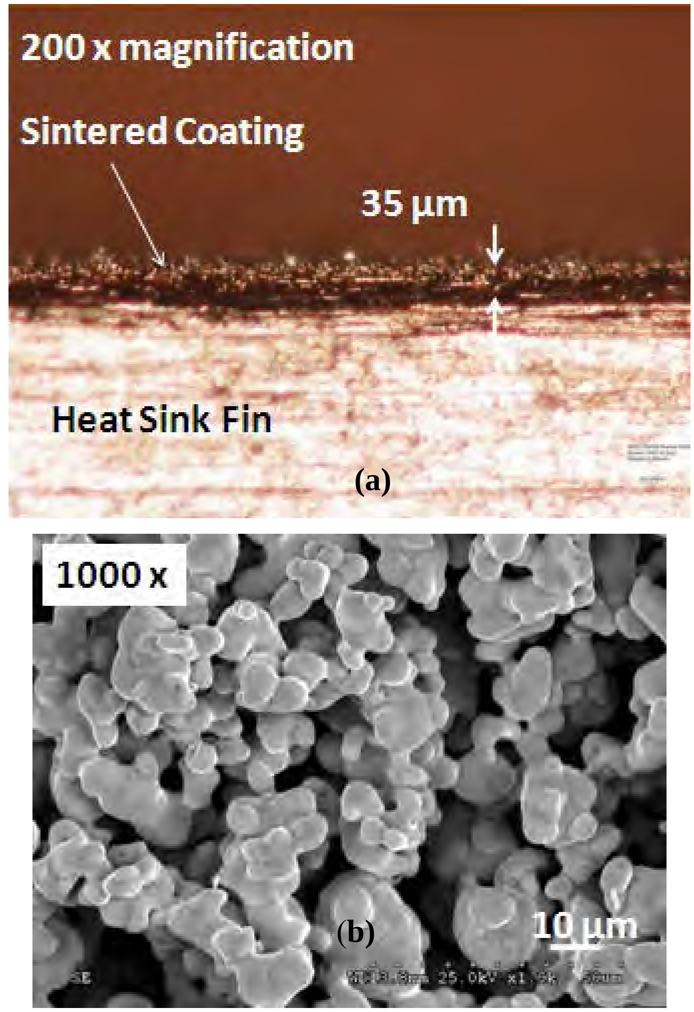

Figure 3: Sintered coating 1 on a copper heat sink fin; (a) 200-times magnification, (b) 1000-times magnification

The average coating thickness was around 35 µm. As shown, the average pore size ranges approximately from 5 to 15 µm and provides a high density of nucleation sites for bubble nucleation.

TEST BED AND TEST SECTION

A two-phase pumped loop test bed for testing heat sinks with and without the porous coating was designed and built. A layout of the test loop is shown in Figure 4.

The test bed is composed of a test section, a condenser with a cooling bath, a DC pump (Fluid-O-Tech MG213XPB17), a single phase flow filter or filter 1 (440 µm) and a flowmeter 1 (McMillan 104-8E, ± 0.05 LPM), a two-phase flow filter or filter 2 (15 µm) and a flowmeter 2 (McMillan 104-5E, ± 0.005 LPM) in parallel to the single phase flow meter and the filter, a pre-heater with a PID controlled power supply, and a two-phase reservoir to regulate the loop pressure (by adjusting the temperature of the reservoir). A charging port was placed before the pump and used to evacuate and charge the loop. The loop was also instrumented with several T-type thermocouple probes (Omega TJC48-CPSS-062G-2) that were inserted into the refrigerant lines. All the loop components were well insulated using silicon foam insulation.

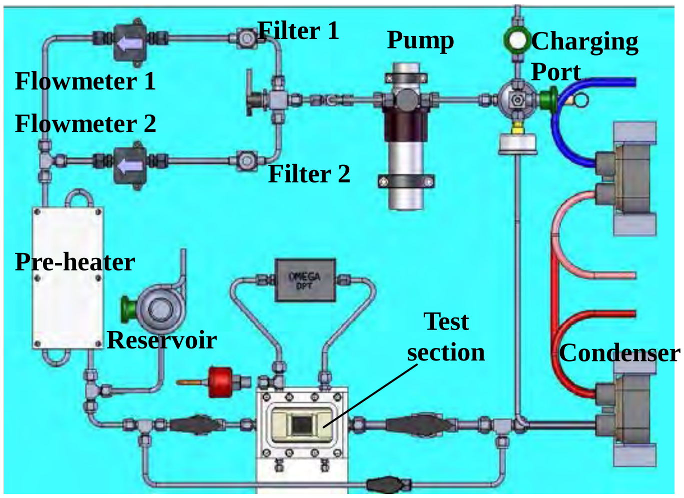

Figure 4: A layout of the test bed for testing heat sinks

Several factors were considered during the design of the test section. The test section had to ensure a simple installation of the heat sink and to provide temperature measurements of the heat sink base as well as temperature and pressure measurements of the refrigerant at the inlet and outlet of the heat sink. Furthermore, the test section had to provide visual access to the boiling process inside the heat sink. A cross-section view of the test section with a heat sink is provided in Figure 5. The test section housing was fabricated from high temperature resistant PolyEther-Ether-Ketone (PEEK) plastics. The heat sink was inserted into the PEEK housing. A silicon o-ring was inserted into a groove formed in the PEEK to seal the heat sink from the ambient. Borosilicate glass was placed atop the heat sink and compressed against the PEEK housing with an aluminum flange to provide visual access to the heat sink channels. A second o-ring was used to seal the gap between the borosilicate glass and the PEEK housing. A copper block with two 500 W cartridge heaters was used to simulate the heat source.

To obtain an accurate measurement of the amount of heat that was conducted into the heat sink, three holes were drilled into the pedestal of the heater with a depth of 7.87 mm and a distance from each other 3.18±0.05 mm. Three T-type thermocouples were inserted into the holes and the measurements of the three temperatures were used to calculate the heat flux. A spring-loaded bolt with a swivel pad was used to uniformly press the heater against the heat sink. Shin-Etsu G-751 thermal interface material was applied on the interface between the heat sink and the heater block to minimize thermal interface resistance. Four thermocouples with a solid ceramic insulation were made and inserted through the heater block and pressed against the heat sink base. The thermocouples were located 7.6 mm from the edge of the heat sink and 0.5 mm underneath the channels. It is believed that the thermocouples were close enough to the heat sink channels so that variations in refrigerant flow could be registered. A thermocouple (Omega TJC48-CPSS-062G-2) and an absolute pressure transducer (Omega PX481AD-100-G5V, ±0.1 PSI) were placed at the inlet to the heat sink and another thermocouple and absolute pressure transducer were placed at the outlet of the heat sink. In addition, a differential pressure transducer (Omega PX2300-25DI, ± 0.06 PSI) was connected between the inlet and the outlet of the heat sink. The heater block was well insulated using amorphous silica blanket with thermal conductivity 0.02 W/m K.

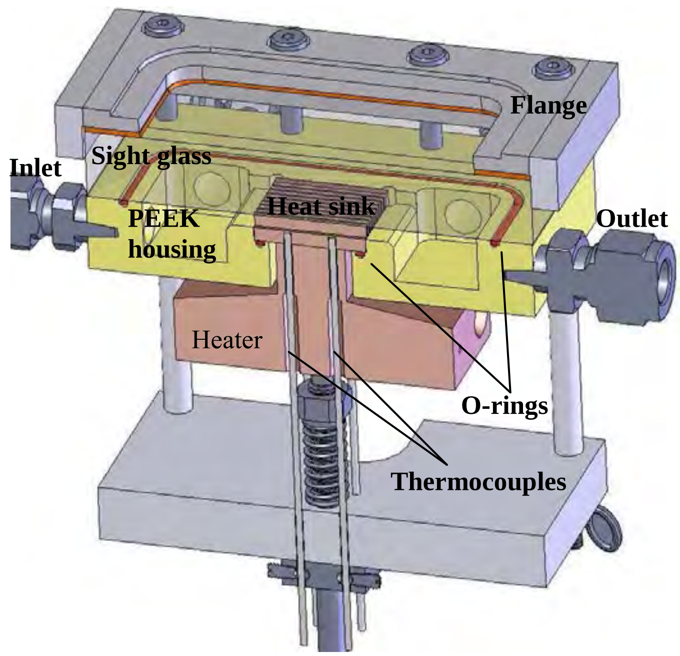

Figure 5: Test section with the heat sink (cross-section view)

All the heat sinks were fabricated from C1100 copper by CNC milling. Six of the heat sinks were coated with microporous coating and two remained uncoated as indicated in Table 1. A photograph of two of the heat sinks is shown in Figure 6.

Before proceeding with the test, the test loop was evacuated to < 0.13Pa (10^{-3} torr) and charged with degassed R245fa refrigerant. The level of dissolved gas in the refrigerant was < 5 ppb. No additional degassing of the refrigerant was required. During the operation, the heat from the heater block vaporized a portion of the refrigerant. A two-phase refrigerant was condensed and subcooled in the condenser. Subcooled liquid entered the pump and was pumped through the filter, flowmeter and then pre-heater. The pre-heater reduced the amount of subcooling to <3 °C subcooling. Slightly subcooled liquid entered the test section which contains the heat sink. Temperatures, pressures, and flow rates were recorded at a sampling rate of 1 Hz.

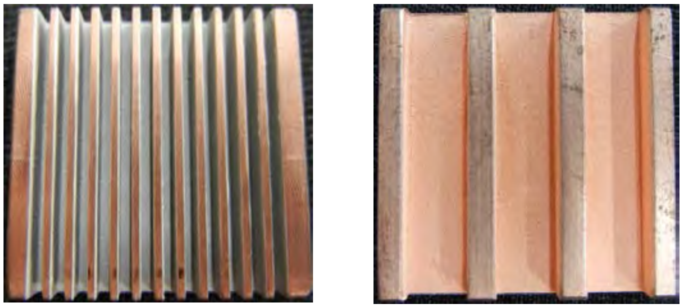

Figure 6: Heat sink 2 (left) and heat sink 6 (right)

RESULTS AND DISCUSSION

Before proceeding with two-phase heat sink tests, a series of single phase heat sink tests were completed to verify the operation of the test bed. The heat applied to the heat sink was calculated from measured current and voltage (the accuracy of the measurement is estimated to be ±3%). The heat load calculated from voltage and current was in average 5% higher than the heat load calculated from the heat conduction through the heater pedestal. The difference was due to heat losses through the insulation. The amount of heat absorbed by the refrigerant and the amount of heat removed at the condenser were calculated to be less than 3% different from the amount of heat applied to the heat sink. These results confirmed that the test loop was well insulated and that the accuracy of the heat load calculated from the conduction through the pedestal was better than 3%. After verifying the conservation of energy with the single phase flow, two-phase tests at various conditions were then performed.

After starting the two-phase tests with heat sink 1, significant compressible volume instabilities were observed [11, 12, and 13]. To eliminate this type of instability, the valve at the inlet to the test section was slightly closed. This additional flow resistance at the inlet to the test section was sufficient to suppress the compressible volume instability without measureable increase in the pumping power.

After eliminating the instabilities caused by the two-phase reservoir upstream of the test section, tests were performed with different heat sinks. The heat sinks were tested at various heat fluxes and a constant flow rate. An example of the refrigerant temperatures at different heat fluxes is given in Figure 7.

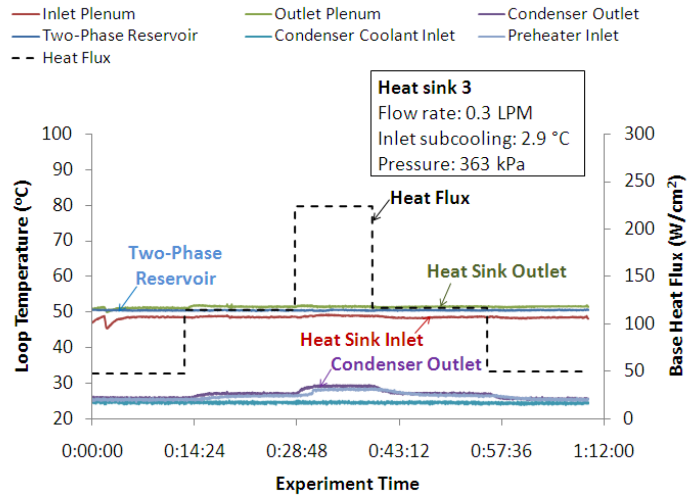

Figure 7: Loop temperatures for heat sink 3

As shown, the refrigerant temperatures at the inlet and outlet of the test section remained steady during the test. This was achieved by controlling the temperature of the two-phase reservoir. As the heat load increased and more vapor was produced, the excess liquid was displaced into the reservoir. The condenser outlet temperature also increased as the heat flux increased. The reason for this can be understood as follows: as more heat was applied to the heat sink, more vapor was generated and a larger portion of the condenser surface was then used to condense the vapor; thus, the condenser area available to subcool the liquid was reduced. The inlet temperature was subcooled in average for 2.9 °C. The average refrigerant temperature at the outlet of the heat sink was 51.6 °C and the average refrigerant pressure at the outlet of the heat sink was measured to be 362.7 kPa. The saturation temperature for R245fa at 362.7 kPa is exactly 51.6 °C (NIST REFPROP 8.0). The average condenser outlet temperature was 26.8 °C meaning that the condenser subcooled the refrigerant an average of 24.8 °C. The pre-heater reduced the amount of subcooling to 2.9 °C. Subcooling the refrigerant less than 2-3 °C is very difficult to achieve since the pre-heater setting with subcooling less than 2 °C easily results in boiling of the refrigerant within the pre-heater.

Heat sink 1 was tested at a flowrate of 0.3 LPM and at base heat fluxes that ranged from 0 to 214 W/cm^2 (and back to 0 W/cm^2). The base heat flux was defined as the heat flux into the heat sink base while the wall heat flux was defined as the heat flux into the refrigerant (from the heated wall). For discrete base heat fluxes within this range, the refrigerant pressures at the inlet and the outlet were recorded at a sampling rate 1 Hz and are presented in Figure 8.

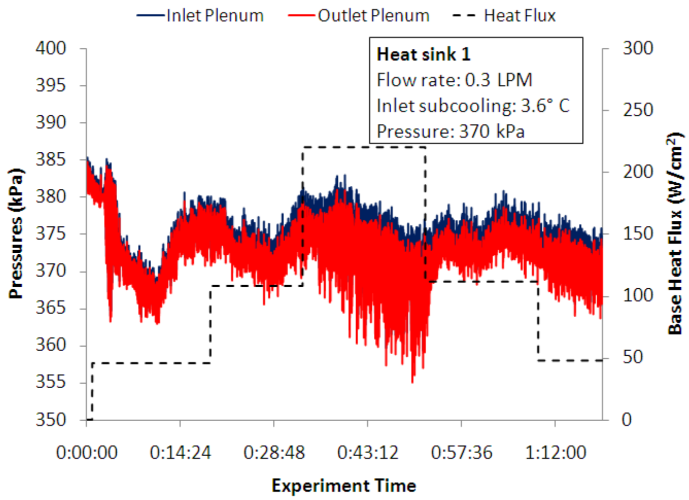

Figure 8: Inlet and outlet pressures for heat sink 1 (1Hz sampling rate)

The oscillations in pressure are clearly present; however, they significantly affect the heat sink base temperature only at heat fluxes above ~ 150 W/cm^2 as shown in Figure 9. Thermocouples TC1 to TC4 were located underneath the heat sink 7.6 mm from the edge of the heat sink and 0.5 mm underneath the channels. (In Figure 9, the thermocouple TC4 readings overlap the rest of the thermocouple readings at 214 W/cm^2.)

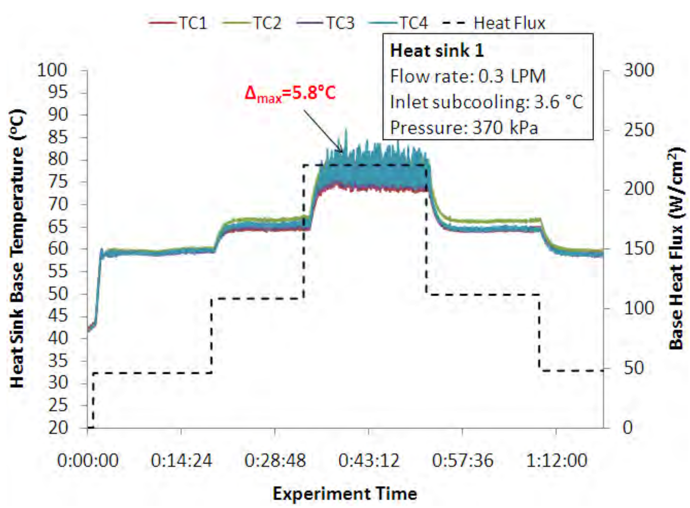

Figure 9: Heat sink base temperatures for heat sink 1 (1Hz sampling rate)

The maximum amplitude of oscillations in the heat sink base temperature was 5.8 °C. The oscillations in heat sink base temperature represent the oscillations in the temperature of the device being cooled. Temperature oscillations of 6 °C are relatively high and are not desirable for cooling electronics components.

After testing heat sink 1, heat sinks 2 and 3, with different types of microporous coatings were also tested. Heat sinks 2 and 3 were tested at exactly the same test conditions as heat sink 1. For heat sink 3, the results for the refrigerant pressures at the inlet and the outlet are presented in Figure 10 and the heat sink base temperatures in Figure 11.

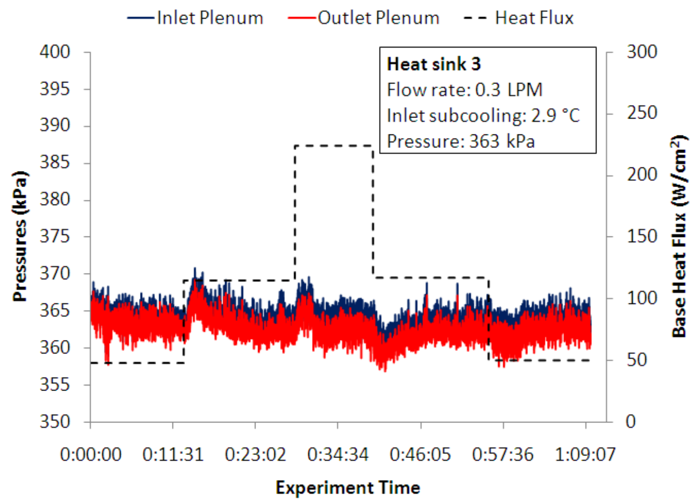

Figure 10: Inlet and outlet pressures for heat sink 3 (1Hz sampling rate)

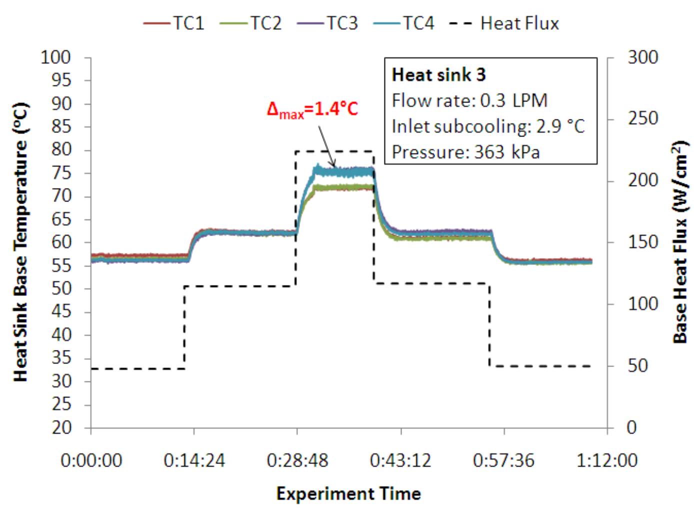

Figure 11: Heat sink base temperatures for heat sink 3 (1Hz sampling rate)

For heat sink 3, the amplitude of the pressure oscillations is smaller than that for heat sink 1 and the maximum amplitude of the oscillations in the heat sink base temperature is only 1.4 °C (compared with 5.8°C for the uncoated sample). Similar results were obtained for heat sink 2. Heat sinks with porous coating on the channel walls therefore result in more stable operation and have smaller temperature oscillations. Cooling an electronic device with a maximum heat sink temperature oscillation of ~1 °C is much more desirable. For completeness, some discrepancies were noted in the temperatures measured at different locations on the heat sink. The test was therefore repeated several times and it was found that the differences were due to the thermocouple contact resistances. Therefore, it is believed that the actual difference in heat sink base temperature is even smaller than it appears in Figure 11. For reference, the model predicts that the temperature of the heat sink base varies only 1 °C at 225 W/cm^2.

Heat transfer performances of heat sinks 1 to 3 were compared in terms of heat sink thermal resistance and pressure drop through the heat sink. Four steady state heat sink base temperatures were averaged over a period of 60 seconds and subtracted from the average refrigerant inlet and outlet temperature and divided by the base heat flux, both also averaged over a period of 60 seconds. The steady state was assumed when the temperature did not change for more than 1 °C in 10 minutes. The comparison is presented in Figure 12.

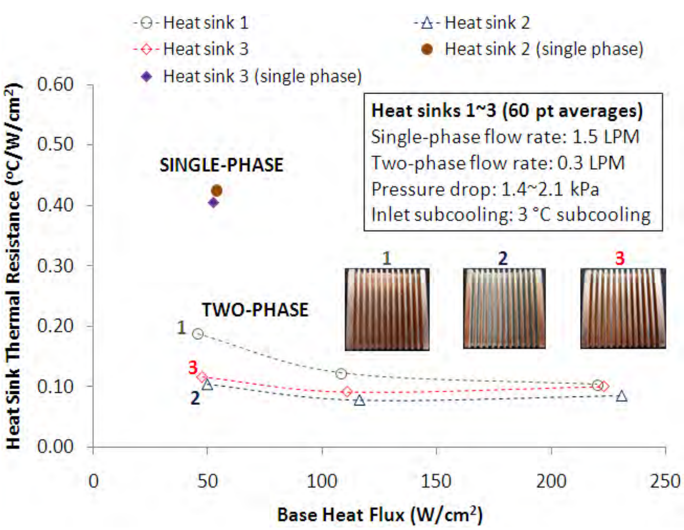

Figure 12: Heat sink thermal resistance versus base heat flux for heat sinks 1 to 3

For all heat sinks, the thermal resistance decreases with increasing heat flux up to ~100 W/cm^2. To better understand this behavior, the model was used to predict the heat sink performance. For example, the average heat transfer coefficient along the channel at 50 W/cm^2 was computed to be 4188 W/m^{2}K while the heat transfer coefficient at 200 W/cm^2 increased to 8264 W/m^{2}K. One of the simplest explanations for this increase is that as the vapor void increases and the vapor slugs move downstream the channel, a thin liquid film forms on the wall. As the heat flux increases, the vapor void increases and the liquid film thickness decreases. Since the heat transfer coefficient is inversely proportional to the thickness of the liquid film, it increases as the film thickness decreases.

Figure 12 also includes the heat sink thermal resistances for two of the heat sinks tested in the single phase flow regime. The thermal resistance for heat sink 2 at a base heat flux of 50 W/cm^2 and single phase flow was 0.425 °C-cm^2/W. For the same heat sink tested at the same heat flux, the thermal resistance was reduced to 0.104 °C-cm^2/W as the flow regime changed from a single phase flow to a two-phase flow. For example, at a base heat flux of 50 W/cm^2, if the heat sink base temperature is to be maintained at 50 °C, a single phase loop will require a coolant at 29 °C while a two-phase loop could use a coolant with a temperature of 45°C. In addition, the flow rate for the two-phase flow was 5-times lower than for the single phase flow, which translates into a significant reduction in the pumping power, which directly depends on the flowrate.

A comparison of the thermal resistances of the three heat sinks clearly shows that the heat sinks with the porous coating result in a lower thermal resistance at all heat fluxes. The largest difference occurs at the lower heat fluxes. Ammerman and You [23] observed that boiling surfaces with microporous coating have a higher number of nucleation sites and higher bubble departure frequency. They have observed using FC-72 and a microporous coating that as initial vaporization occurred within the microporous coating, the embryonic bubble grew rapidly and vapor generated from one individual liquid-vapor interface was divided into many tiny bubbles (<0.2 mm). The resulting effect at low heat fluxes is high bubble departure frequency and small bubble departure diameter. For an uncoated surface, they observed bubble departure diameter of 0.7 mm and also the incipient superheat to initiate the vaporization was higher. Similarly, we could expect that the heat sinks 2 and 3 with porous coating will start nucleating bubbles at lower superheat resulting in significantly lower thermal resistance at low heat fluxes. Also since the bubble departure diameter that nucleates on a microporous coating is smaller, the bubbles are less likely to be radially restricted inside the heat sink channels resulting in more stable operation with less oscillation in pressure.

A pressure drop through the heat sinks at different heat fluxes was also measured and it ranged from 1.4 to 2.1 kPa. No measureable difference in pressure drops for the different heat sinks was measured. This was expected since addition of the coating does not significantly change the flow cross-sectional area. For reference, the channel hydraulic diameter was 1732 µm while the thickness of the coating was 35 to 45 µm.

Several additional tests were performed using heat sink 3. The heat sink was tested at three different working pressures: 273 kPa, 363 kPa, and 486 kPa, respectively. At each of these pressures, the heat fluxes were varied from zero to the CHF. The results showed no measurable difference in the CHF and the heat sink thermal resistance. Also no differences were observed in the amplitude of heat sink base temperature oscillations at different pressures.

The heat sink was also tested at three different flow rates from 0.15 to 0.45 LPM. It was found that by increasing the flow rate by a factor of three, the thermal resistance was reduced by an average of 11%. By increasing the flow rate from 0.15 LPM to 0.45 LPM, the CHF also increased from 178 W/cm^2 to 267 W/cm^2. The amplitude of temperature oscillations was 1.4 °C at flow rates up to 0.3 LPM and decreased to 0.9 °C at flow rates higher than 0.3 LPM. By increasing the flow rate from 0.15 LPM to 0.45 LPM, the pressure drop through the heat sink also increased by 0.7 kPa.

The effect of the refrigerant subcooling prior to entry into the heat sink was also considered. Increasing the subcooling increased the heat sink thermal resistance. For example, at a base heat flux of 115 W/cm^2, the thermal resistance was 0.141 °C-cm^2/W at an inlet subcooling of 12 °C while the thermal resistance was reduced to 0.093 °C-cm^2/W for an inlet subcooling of 3 °C. It is expected that by having saturated liquid at the inlet to the heat sink with no subcooling, the thermal resistance will be further reduced. By increasing the amount of subcooling from 3 to 12 °C, the heat sink wall temperature did not however decrease. This is because the single phase heat transfer coefficient is several times lower than the two-phase heat transfer coefficient. In terms of the CHF, increasing the subcooling from 3 °C to 12 °C resulted in an increase in CHF from 246 W/cm^2 to 274 W/cm^2. The amplitude of the heat sink base temperature oscillations at subcooling 8 °C and 12 °C was 1.1 °C while it was slightly increased to 1.4 °C as the inlet subcooling decreased to 3 °C.

Heat sinks 4 to 8 were tested at two different flow rates, 0.3 LPM and 0.6 LPM, and at different heat fluxes. Heat sinks 4 to 8 reached CHF at lower base heat flux than heat sinks 1 to 3. At 0.3 LPM (the same flow rate used to test heat sinks 1 to 3), heat sinks 4, 5, and 6 reached the CHF at a wall heat flux of ~23 W/cm^2 while heat sinks 7 and 8 reached the CHF at wall heat flux ~40 W/cm^2. For reference, heat sinks 1 to 3 reached CHF at wall heat flux of ~23 W/cm^2. Since heat sinks 1 to 3 had a total wetted area that was 2.5-times higher than heat sinks 4 to 6, they were able to handle 2.5-times higher base heat fluxes (by only considering uncoated heat sinks and neglecting the increase of the wetted area due to the porous coating). For heat sinks 4 to 8, the oscillations in pressure were similar to oscillations in pressure for heat sink 3 shown in Figure 10, while the oscillations in temperature were reduced to ±0.25 °C. This was expected since the channel hydraulic diameter was larger than for heat sinks 1 to 3 and the bubbles were not radially restricted by the channel walls.

The summary of the test results at 0.3 LPM for heat sinks 4 to 8 are presented in Figure 13. The thermal resistance decreases with increasing heat flux for all of the heat sinks, similar to the results obtained with heat sinks 1 to 3 reported above. There is however an even more significant improvement in terms of the reduction in the heat sink thermal resistance (or increasing heat sink heat transfer coefficient) for heat sinks with the porous coating. Regarding the thermal resistance, the lowest thermal resistance was measured for heat sink 7 and the second lowest thermal resistance was measured for heat sinks 6 and 8. Heat sink 5 had the highest thermal resistance which was still lower than that associated with the uncoated heat sink (heat sink 4). The highest heat flux was achieved with heat sink 8 and the second highest with heat sink 7. Interestingly, heat sink 7 did not achieve as high of a heat flux as heat sink 8. With respect to the pressure drops, there was no measurable difference between the heat sinks as previously noted. The trend in heat sink thermal resistance vs. heat flux at 0.6 LPM was similar to the results obtained at 0.3 LPM; however, both heat sinks 7 and 8 reached the same CHF at base heat flux of ~175 W/cm^2 (or wall heat flux ~ 45 W/cm^2). Similar to results at 0.3 LPM there was significant reduction in thermal resistance for heat sinks with microporous coating. Also there was no measurable difference in pressure drops for heat sinks 4 to 8 tested at 0.6 LPM.

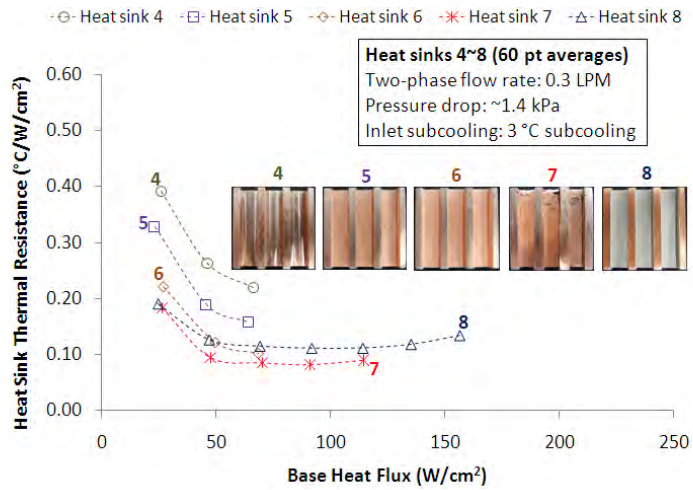

Figure 13: Heat sink thermal resistance versus base heat flux for heat sinks 4 to 8

One very important finding can be seen by comparing performance of heat sink 1 in Figure 12 to heat sink 7 in Figure 13. Heat sink 1 has four times smaller channels that are more expensive to manufacture and are more prone to clogging than heat sink 7. Furthermore, heat sink 7 has lower thermal resistance at base heat fluxes ~ 100 W/cm^2 and significantly lower oscillations in heat sink base temperatures than heat sink 1. Adding microporous coating on heat sink channels was therefore proven to reduce temperature oscillations by minimizing parallel channel instabilities and also enabled using heat sinks with larger channels that are less susceptible to rapid bubble growth instability.

CONCLUSIONS

Three mini-channel heat sinks with twelve rectangular channels, a hydraulic diameter of 1.7 mm, and a channel aspect ratio of 2.7, and five small-channel heat sinks with three rectangular channels, a hydraulic diameter of 4.1 mm, and a channel aspect ratio of 0.6 were fabricated. All heat sinks had overall dimensions 25.4 mm x 25.4 mm x 6.4 mm. Two different metal powder coatings were developed and deposited on six of the heat sinks as listed in Table 1. A two-phase test bed loop was designed and built. The heat sinks were tested with degassed R245fa refrigerant at various heat fluxes, flow rates, system pressures, and various degrees of refrigerant subcooling. The following can be concluded from this research:

- Parallel channel instabilities were significantly less pronounced with heat sinks with the porous coating. Adding microporous coating on mini-channel heat sinks suppressed the instabilities and reduced the amplitude of temperature oscillations from 6 °C to slightly more than 1 °C.
- Adding a microporous coating on the channel walls did not increase the pumping power or pressure drop

through the heat sink for any of the tested heat sinks.

- Mini-channel heat sinks with porous coating (heat sink 2 and 3) resulted in average 1.5-times higher heat transfer coefficient than that of the uncoated mini-channel heat sink (heat sink 1).
- Small-channel heat sinks with porous coating (heat sinks 5 to 8) had in average 2.5~2.7-times higher heat transfer coefficient and 1.5~2-times higher critical heat flux than the uncoated heat sink (heat sink 4).
- Heat sinks with large channels and optimized porous coating (heat sink 7 and 8) can remove heat at the same or lower heat sink thermal resistance and are significantly more stable (improved temperature uniformity of ±0.5°C) than the heat sinks with almost four times smaller channels without the porous coating (heat sink 1).

ACKNOWLEDGMENTS

This work was performed under NSF SBIR Phase I program (Award ID.: 1013608). The program director was Dr. Muralidharan S. Nair. The authors would like to thank to Dr. Howard Pearlman and Dr. Xudong Tang from ACT for their suggestions and support during the program. The contributions of ACT's personnel Mr. Andrew Radesky and Mr. Jeff Reichl are greatly appreciated. The authors would also like to thank to Dr. Ajay Gurung and Dr. Miguel Amaya for help with the ABM coating.

REFERENCES

[1] Ledinegg, M., 1938, "Instability of flow during natural and forced circulation, *Wärme* **61** (8) 891-898

[2] Bouré, J.A., Bergles, A.E., Tong, L.S., 1973 "Review of two-phase flow instabilities," *Nuclear Eng. Des.* **25** 165-192

[3] Bergles, A. E. and Kandlikar, S.G., 2005, "On the Nature of Critical Heat Flux in Microchannels," *J. of Heat Transfer* **127** (10) 101-107.

[4] Hetsroni, G., Mosyak, A., Segal, Z., Pogrebnyak, E., 2003, " Two-phase flow patterns in parallel micro-channels," *Int. J. of Multiphase Flow* **29** 341-360.

[5] Hetsroni, G., Mosyak, A., Segal, Z., Pogrebnyak, E., 2005, " Explosive boiling of water in parallel micro-channels," *Int. J. of Multiphase Flow* **31** 371-392.

[6] Chang, K.H., Pan, C., 2007, "Two-phase flow instability for boiling in a microchannel heat sink," *Int. J. Heat Mass Transfer* **50** 2078-2088

[7] Koşar, A., Kuo, C.-J., Peles, Y., 2006, " Suppression of Boiling Flow Oscillations in Parallel Microchannels by Inlet Restrictors, "*J. of Heat Transfer* **128** 251-260

[8] Zuber, N., 1959, "Hydrodynamic aspects of boiling heat transfer," AECU-4439, *Physics and Mathematics*, US Atomic Energy Commission

[9] Collier, J.G., Thome, J.R., 1994, *Convective Boiling and Condensation*, third ed. Oxford University Press, Oxford

[10] Kandlikar S.G., 2002, "Fundamental issues related to flow boiling in minichannels and microchannels," *Exp. Thermal and Fluid Science* **26** 389-407

[11] Qu, W., Mudawar, I., 2003, "Flow boiling heat transfer in two-phase micro-channel heat sinks-I. Experimental investigation and assessment of correlation methods," *Int. J. Heat Mass Transfer* **46** 2755-2771

[12] Qu, W., Mudawar, I., 2005, "Measurement and correlation of critical heat flux in two-phase micro-channel heat sinks," *Int. J. Heat Mass Transfer* **47** 2045-2059

[13] Lee H .J., Yao, S .-C., 2009, " System Instability of Evaporative Micro-Channels," ASME Paper HT2009-88217

[14] Agostini, B., Thome, J., R., Fabbri, M., Michael, B., Calmi, D., Kloter, U., 2008, "High heat flux flow boiling in silicon multi-microchannels-Part I : Heat transfer characteristics of refrigerant R236fa," *Int. J. of Heat and Mass Transfer* **51** 5400-5414

[15] Wang, G., Cheng, P., Bergles, A., E., 2008, " Effects on inlet/outlet configurations on flow boiling in stability in parallel microchannels," *Int. J. of Heat and Mass Transfer* **51** 2267-2281

[16] Koşar, A., Kuo, C., J., Peles, Y., 2005, "Reduced Pressure Boiling Heat Transfer in Rectangular Microchannels With Interconnected Reentrant Cavities," *J. of Heat Transfer* **127** 1106-1114.

[17] Kuo, C.-J., Peles, Y., 2008, "Flow Boiling Instabilities in Microchannels and Means for Mitigation by Reentrant Cavities," *J. of Heat Transfer* **130** 072402-1 – 072402-10.

[18] David, M., P., Khurana, T., Hidrovo, C., Pruitt, B., L., Goodson, K., E., 2007, " Vapor-Venting, Micromachined Heat Exchanger for Electronics Cooling," ASME Paper IMECE2007-42553

[19] Zhang, W., Hibiki, T., Mishima, K., 2004, " Correlation for flow boiling heat transfer in mini-channels," *Int. J. of Heat and Mass Transfer* **47** 5749-5763

[20] Trautman, M .A., Tirumala, M ., You, S .M., 2008, "Investigation of Microporous Coatings and Mesoscale Evaporator Enhanacement for Two-Phase Cooling of Electronic Components," *J. of Electronic Packaging* **130** 011007-1-011007-6

[21] You, S., M., Rainey, K., N., Ammerman, C., N., 2004, "A New Microporous Surface Coating for Enhancement of Pool and Flow Boiling Heat Transfer," *Adv. in Heat Transfer* **38** 73-141

[22] You, S., M., O'Connor, J. P., 1998, "Boiling Enhancement Coating," US Patent 5,814,392

[23] Ammerman, C.N. and You, S .M., 2001, " Enhancing Small-Channel Convective Boiling Performance Using a Microporous Surface Coating," *J. of Heat Transfer* **123** pp. 976-983.

